ISSN 0006-3509, Biophysics, 2022, Vol. 67, No. 6, pp. 902–912. © Pleiades Publishing, Inc., 2022.
Russian Text © The Author(s), 2022, published in Biofizika, 2022, Vol. 67, No. 6, pp. 1109–1121.

MOLECULAR BIOPHYSICS

# SARS-COV-2 Coronavirus Papain-like Protease PLpro as an Antiviral Target for Inhibitors of Active Site and Protein–Protein Interactions

**P. V. Ershov[a,*], E. O. Yablokov[a], Y. V. Mezentsev[a], G. N. Chuev[b], M. V. Fedotova[c], S. E. Kruchinin[c], and A. S. Ivanov[a]**

[a] *Institute of Biomedical Chemistry, Moscow, 119121 Russia*

[b] *Institute of Theoretical and Experimental Biophysics, Russian Academy of Sciences, Pushchino, Moscow oblast, 142290 Russia*

[c] *Krestov Institute of Solution Chemistry, Russian Academy of Sciences, Ivanovo, 153045 Russia*

**e-mail: pavel79@inbox.ru*

Received June 5, 2022; revised August 9, 2022; accepted August 12, 2022

**Abstract**—The papain-like protease PLpro of the SARS-CoV-2 coronavirus is a multifunctional enzyme that catalyzes the proteolytic processing of two viral polyproteins, pp1a and pp1ab. PLpro also cleaves peptide bonds between host cell proteins and ubiquitin (or ubiquitin-like proteins), which is associated with a violation of immune processes. Nine structures of the most effective inhibitors of the PLpro active center were prioritized according to the parameters of biochemical ($IC_{50}$) and cellular tests to assess the suppression of viral replication ($EC_{50}$) and cytotoxicity ($CC_{50}$). A literature search has shown that PLpro can interact with at least 60 potential protein partners in cells, 23 of which are targets for other viral proteins (human papillomavirus and Epstein-Barr virus). The analysis of protein–protein interactions showed that the proteins USP3, UBE2J1, RCHY1, and FAF2 involved in deubiquitinylation and ubiquitinylation processes contain the largest number of bonds with other proteins; the interaction of viral proteins with them can affect the architecture of the entire network of protein–protein interactions. Using the example of a spatial model of the PLpro/ubiquitin complex and a set of 154 naturally occurring compounds with known antiviral activity, 13 compounds (molecular masses in the range of 454–954 Da) were predicted as potential PLpro inhibitors. These compounds bind to the "hot" amino acid residues of the protease at the positions Gly163, Asp164, Arg166, Glu167, and Tyr264 involved in the interaction with ubiquitin. Thus, pharmacological effects on peripheral PLpro sites, which play important roles in binding protein substrates, may be an additional target-oriented antiviral strategy.

**Keywords:** SARS-CoV-2, papain-like protease, PLpro, protein–protein interactions, virus-host, surface plasmon resonance, inhibitors

**DOI:** 10.1134/S0006350922060082

## INTRODUCTION

On March 11, 2020, the World Health Organization announced the beginning of the COVID-19 pandemic, which was caused by the SARS-CoV-2 coronavirus. The disease has put a serious strain on national health systems and led to the death of several million people worldwide [1]. Even before the outbreak of the omicron strain (B.1.1.529), by mid-November 2021, more than 40% of the world's population had been infected with COVID-19 at least once [2]. The emergence and rapid spread of new strains of SARS-CoV-2 stimulated the development of drugs that block different stages of the life cycle of the virus. This is also achieved by inhibiting key enzymes of the viral replication apparatus [3].

The papain-like protease (PLpro) and the main protease (Mpro) of SARS-CoV-2 carry out the proteolytic cleavage of two viral polyproteins, pp1a and pp1ab, which is important for the maturation of 16 proteins involved in the replication and assembly of viral particles [4]. PLpro is a monomeric protein with a multidomain structure (Fig. 1) and a "catalytic triad" (amino acids Cys112, His273, and Asp287) in the active center, which recognizes and cleaves the Leu-

*Abbreviations*: PLpro, papain-like protease of SARSCoV-2; Mpro, main protease of SARS-CoV-2; PPI, protein–protein interactions; SPR, surface plasmon resonance; a.a.r., amino acid residues.

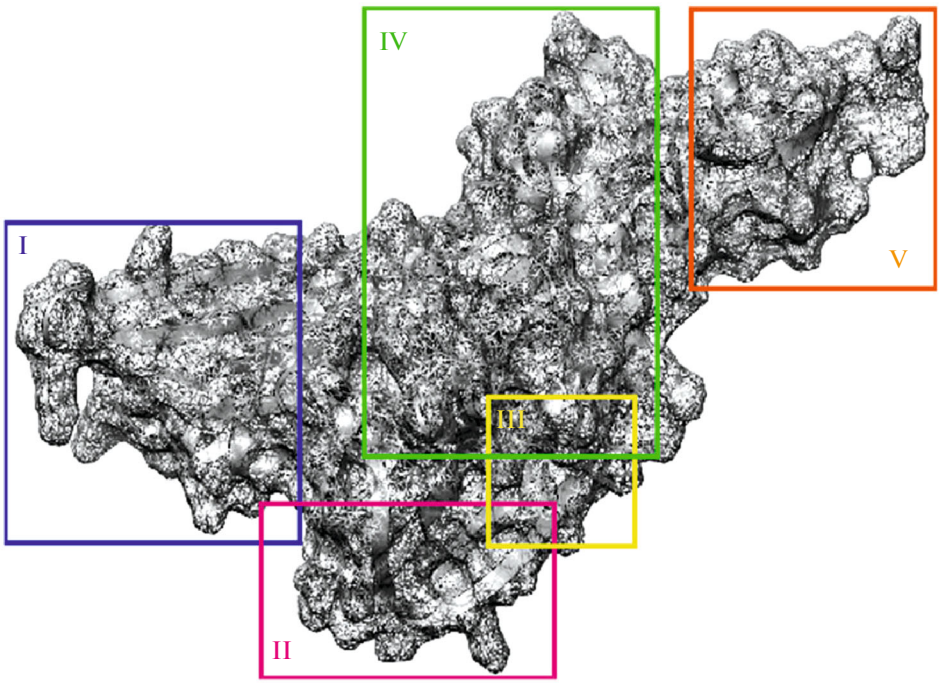


**Fig. 1.** Crystallographic structural model of SARS-CoV-2 PLpro (PDB ID 7cmd [6]). Roman numerals in the figure indicate: I, Zn-binding domain (one zinc ion is coordinated by four cysteine residues, Cys189, Cys192, Cys224, and Cys226); II, Palm domain; III, catalytic triad, Cys111–His272–Asp286; IV, Thumb domain; V, ubiquitin-like domain.

X-Gly-Gly polyprotein motif (where X is any amino acid residue) to form viral proteins nsp1, nsp2, and nsp3 [5].

To date, there are no PLpro inhibitors approved for clinical use. According to the Clinical Trials portal, clinical trials are being conducted on two candidate inhibitors of PLpro, isotretinoin (NCT04361422) and ebselene (NCT04484025). The vast majority of scientific developments were devoted to the identification of reversible and irreversible inhibitors targeted specifically at the active center of the viral enzyme. In parallel with the generation of a large amount of information about new PLpro inhibitors, it should be noted that the number of bioinformatic hypotheses predicted in silico [7–11] may exceed the number of experimentally verified inhibitors by approximately an order of magnitude. This fact gives rise to an obvious problem meaning that not all hypotheses are productive [12, 13]. In this context, the use of multimethodic tools (biochemical tests, assessment of binding capacity, and cellular tests) is a reference option for prioritizing new SARS-CoV-2 PLpro inhibitors [14–16]. However, it is appropriate to note that the pharmacological effect on the active center of PLpro has some biological limitations. Firstly, the occurrence of amino acid substitutions in the active center due to the high mutational variability of different strains of the virus can quickly form resistance to competitive inhibitors. Secondly, the wide representation of Cys residues in the active centers of cellular enzymes increases the likelihood of nonselective action of inhibitors forming covalent bonds with Cys.

The peculiar feature of PLpro to interact with cellular proteins emphasizes the multifunctional aspect of the enzyme. It was found that this phenomenon is accompanied by the cleavage of peptide bonds between labelled proteins (ubiquitin, ISG15, interferon-stimulated gene 15, and ubiquitin-like protein Nedd8) and target proteins [16–18]. PLpro indirectly affects the expression of the interferon gene (IFN) by reducing the level of ubiquitinylation of TRAF3, TBK1, IKK1, STING, and IRF3 proteins [19]; thereby it disrupts the course of immune processes and the ability of PLpro to participate in protein–protein interactions (PPI) [20]; this allows it to be generally considered as an exogenous modulator of cellular signaling pathways through a change in the PPI spectrum. As will be shown later, a conservative region adjacent to the active center of the viral enzyme is apparently involved in the PPI of PLpro and cellular proteins; therefore, an alternative strategy to reduce the toxic effect of PLpro on the human body could be implemented by the pharmacological blockade of PPI in the coordinates of the virus-host.

One of the aims of this study was to review the most promising and experimentally verified candidate inhibitors of SARS-CoV-2 PLpro discovered to date. The second aim was to systematize data on PLpro interactomics and discuss the possibilities of blocking

PPI with PLpro by low-molecular compounds with known antiviral activity.

## EXPERIMENTAL VERIFICATION OF PREDICTED IN SILICO INHIBITORS

Surface plasmon resonance (SPR) is one of the methods of experimental verification of potential PLpro inhibitors predicted in silico. SPR analysis makes it possible to determine the kinetic, equilibrium, and thermodynamic constants of intermolecular interaction. In the studies where the SPR biosensor was used, a recombinant full-size PLpro preparation was covalently immobilized on the CM5 optical chip via free amino groups of the protein [14] or via an affine polyhistidine tag [15]. The level of immobilization of PLpro was 12000–13000 RU (resonance unit). The control inhibitor GRL0617 was used as a positive control of binding to PLpro.

In biochemical tests, the kinetics of the PLpro enzymatic reaction was studied in the absence (control) and presence of different concentrations of potential inhibitors to determine $IC_{50}$ values. The parameters of the biochemical test (pH and ionic strength of the buffer solution, the ratio of enzyme and inhibitor concentrations, incubation time, temperature, and the presence of additives) differed significantly, which follows from the analysis of literature sources [15, 21–24]. To detect protease activity, a spectral method based on fluorescent resonance energy transfer (FRET) with fluorescently labeled peptides whose motifs corresponded to PLpro recognition sites, for example, Z-RLRGG-AMC (where AMC is 7-amido-4-methylcoumarin) or Ac-LRGG-ACC (where ACC is 7-amino-4-carbamoyl methylcoumarin), was used. During the proteolytic cleavage of the substrate, a significant increase in the intensity of AMC ($\lambda_{ex}$ = 360 nm; $\lambda_{em}$ = 460 nm) or ACC ($\lambda_{ex}$ = 355 nm, $\lambda_{em}$ = 460 nm) fluorescence was observed; the initial reaction rate ($V_0$) was proportional to the activity of PLpro. To detect the deubiquitinase activity of PLpro, fluorescently labeled protein substrates based on ubiquitin and ISG-15 were used. Buffer solutions contained 20–50 mM tris-HCl (pH 6.8–8.0) with the addition of NaCl to the final concentration of 150 mM. The preincubation time of the inhibitor with PLpro before the addition of the substrate was from 10 to 30 min at room temperature or at 37°C. The final concentrations of PLpro and substrate in the reaction mixture were 10–100 nM and 10–50 μM, respectively; on average, the molar ratio of enzyme to substrate was 1 : 500. The content of additives to improve the solubility of low-molecular-weight compounds in buffer solutions, such as Triton X-100 and dimethyl sulfoxide, was 0.01–0.05% (v/v) and 0–2% (v/v), respectively. The addition of dithiotreitol to the reaction mixture to a final concentration of 3–5 mM was necessary to limit the nonspecific effect of low-molecular compounds on the cysteine residue in the PLpro active center [25]. Six sulfur-containing compounds that had not previously shown inhibition of viral replication but inhibited a number of cysteine proteases in a biochemical test in the absence of dithiotreitol did not reduce the enzymatic activity of proteases in its presence. Just as in the SPR analysis, the control inhibitor GRL0617 ($IC_{50}$ = 0.6 and $K_i$ = 0.5 μM) was used as a positive control. To study the mechanism of inhibition, the target compound in different concentrations was incubated for 30 min in the presence of PLpro (25–150 nM) in a volume of 90 μL. The reaction was started by adding 10 μL of PLpro substrate to a final concentration of 30 μM. The data in the coordinates of the initial velocities and concentrations of PLpro were processed using regression analysis [21].

We performed a search for compounds that were described in the literature simultaneously as inhibitors of the enzymatic activity of PLpro according to the known parameters of $IC_{50}$ and inhibitors of SARS-CoV-2 replication according to the parameters of cytotoxicity ($CC_{50}$) and semimaximal effective concentration ($EC_{50}$). The determination of the parameters of $CC_{50}$ and $EC_{50}$ can be considered more "standardized" due to the use of the same techniques and cellular models (Vero E6, A549, Caco2, and Calu3). As for the $IC_{50}$ values, it is quite difficult to compare them from different studies due to the use of different substrates and the composition of biochemical tests. Figure 2 shows a sample of low-molecular compounds of nonpeptide nature that showed the most favorable inhibition profile according to the parameters $IC_{50}$, $CC_{50}$, and $EC_{50}$: XR8-23 (Fig. 2a) [15], YM155 (Fig. 2b) [26], proanthocyanidin (Fig. 2c) [27], Jun9-75-4 (Fig. 2d) [28], compound 29 (Fig. 2e) [23], compound 6 (Fig. 2f) [29], dihydrotanshinone I (Fig. 2g) [30], tropifexor (Fig. 2h) [31], and compound 7 (Fig. 2i) [32]. An important characteristic of viral enzyme inhibitors is their side effect on cellular targets. Prediction of the spectrum of "nonspecific" cellular targets was performed for six drug-like compounds (Figs. 2b, 2d, 2e, 2f, 2g, 2i) on SwissTargetPrediction [33], BindingDB [34], and TargetNet web servers (ECFP2, ECFP4, ECFP6, and MACCS with AUC = 0.95) [35] with selection hypotheses at the value of the probability score parameter 1. As a result, glycogen phosphorylase was predicted as a potential target for the compounds shown in Figs. 2c, 2f, and 2i; arachidonate-15-lipoxygenase for the compounds shown in Figs. 2d and 2f; calpain-1 and neprilysine for the compounds shown in Figs. 2e and 2i; hepatic carboxyestrase 1 for the compounds shown in Figs. 2f and 2g; and forbolin-1 for the compounds shown in Figs. 2f and 2i. Other protein targets were predicted to be unique for each of the six compounds, and the average number of targets per compound was 12 (range from 3 to 21). Only three "nonspecific" protein targets were predicted for the compound shown in Fig. 2b.

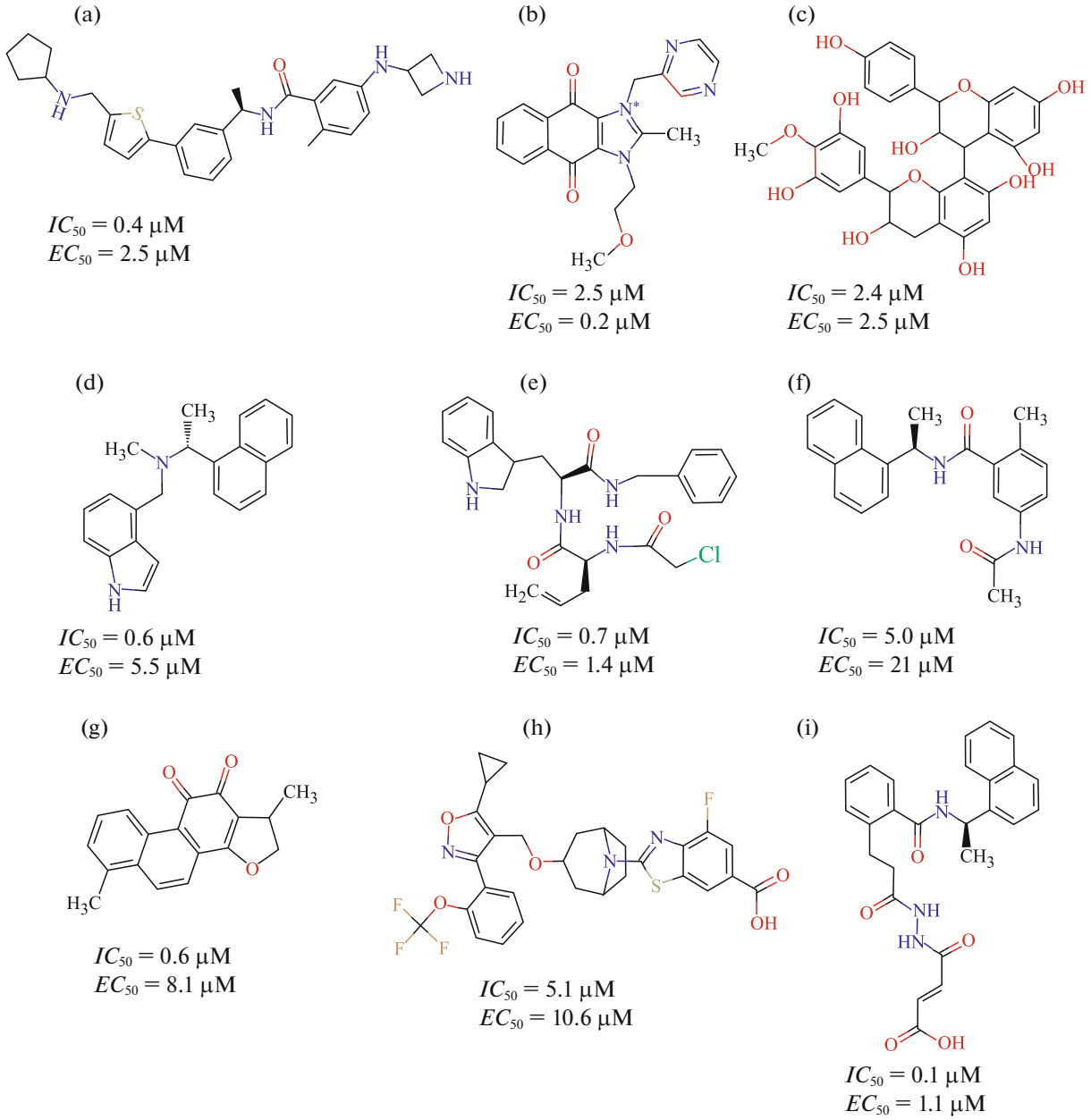


**Fig. 2.** Following compounds are indicated by numbers: (a) XR8-23, (b) YM155, (c) proanthocyanidin, (d) Jun9-75-4, (e) compound 29, (f) compound 6, (g) dihydrotanshinone I, (h) tropifexor, (i) compound 7. Drug-like properties were predicted for compounds (b), (d), (e), (f), (g), and (i), according to the SwissADME resource [36].

## REPOSITIONING OF PHARMACOLOGICALLY ACTIVE COMPOUNDS AS PLpro INHIBITORS

The authors of [37] studied the inhibitory potential of a library of 70 known inhibitors of deubiquitinases and cysteine proteases against SARS-CoV-2 PLpro. It was found that the compounds SJB2–043 (inhibitor of ubiquitin-specific protease 1), TCID (inhibitor of ubiquitin-C-terminal hydrolase L3) and PR-619 (nonselective inhibitor of deubiquitinases) were characterized by $IC_{50}$ values equal to 0.6, 6.4, and 6.1 μM, respectively. When AMC-labeled ubiquitin as a PLpro substrate was used, the $IC_{50}$ value was 0.09 μM in the case of SJB2-043, which binds at the peripheral site of PLpro [37]. Antitumor drug tarloxitinib, an irreversible inhibitor of EGFR and HER2 receptor tyrosine kinases, demonstrated activity against SARS-CoV-2 PLpro ($IC_{50}$ = 0.3 μM and $K_i$ = 0.2 μM, respectively) according to the type of competitive inhibition. In the HUH7 hepatocarcinoma cell model, tarloxitinib reduced the replication of SARS-CoV-2 at a concentration of 10 μM by 25% without showing a significant cytotoxic effect [38]. Losartan, an angiotensin recep-

**Table 1.** Analysis of groups of potential cellular protein targets of SARS-CoV-2 PLpro represented in terms of gene ontology

| Group of gene ontology, $p < 0.05$ | %* | Proteins presented in the group |
|---|---|---|
| GO:0005783 ~ subcellular localization in the endoplasmic reticulum | 57 | ANKLE2, ATL1, FAF2, STX18, UFSP2, AUP1, UBE2J1, UFL1, SMPD4, TMEM43, DDRGK1, ARL6IP5, CLCC1, SEC63, WLS, OSBPL8, CAMLG, MBOAT7, SURF4, CDKAL1, ACSL3, VRK2, TEX2, VMP1, RINT1, LSG1, STIM1, TMEM214, SOAT1, STIM2, REEP4, TRIM13, ESYT2, DHCR7, SLC27A4 |
| GO:0005737 ~ subcellular localization in the cytoplasm | 85 | VEZT, ANKLE2, FMR1, FAF2, UFSP2, AUP1, UFL1, SMPD4, TMEM43, GPBP1, ARL6IP5, CLCC1, SEC63, WLS, CAMLG, AKTIP, USP3, CDKAL1, ACSL3, VRK2, FNDC3A, TEX2, RINT1, LSG1, STIM1, TMEM214, ESPL1, SOAT1, STIM2, TRIM13, SLC27A4, SNAP47, ATL1, STX18, RCHY1, UBE2J1, FXR1, CCNB2, FXR2, DDRGK1, SNX25, OSBPL8, MBOAT7, SURF4, HOOK3, VMP1, TMEM199, SNX19, REEP4, SNX14, ESYT2, DHCR7 |
| GO:0010256 ~ subcellular localization in organelle membranes | 20 | VMP1, OSBPL8, CCNB2, ANKLE2, TMEM43, REEP4, AKTIP, ATL1, SURF4, STX18, ACSL3, HOOK3 |
| GO:0016874 ~ ligase activity | 11 | UFL1, MKRN2, TRIM13, MKRN3, ACSL3, RCHY1, SLC27A4 |
| GO:0035091 ~ involvement in phosphatidylinositol binding | 8 | OSBPL8, SNX19, SNX25, SNX14, ESYT2 |
| GO:0019787 ~ ubiquitin-like transferase activity | 10 | UFL1, ZER1, AKTIP, TRIM13, RCHY1, UBE2J1 |
| GO:0005515 ~ participation in protein binding | 75 | VEZT, SNAP47, ANKLE2, GRAMD1A, TEX264, FMR1, ATL1, FAF2, STX18, UFSP2, AUP1, RCHY1, UBE2J1, FXR1, UFL1, CCNB2, FXR2, TMEM43, DDRGK1, SNX25, GPBP1, ARL6IP5, SEC63, WLS, CAMLG, AKTIP, MBOAT7, USP3, SURF4, CDKAL1, ACSL3, VRK2, HOOK3, VMP1, TMEM199, RINT1, SNX19, STIM1, ESPL1, SOAT1, STIM2, REEP4, TRIM13, MKRN2, MKRN3, ESYT2 |
| GO:0008289 ~ participation in lipid binding | 11 | OSBPL8, SNX19, SOAT1, SNX25, SNX14, ESYT2, TEX2 |
| GO:0005543 ~ participation in phospholipid binding | 8 | OSBPL8, SNX19, SNX25, SNX14, ESYT2 |
| GO:0008017 ~ participation in microtubule binding | 6 | STIM1, REEP4, FMR1, HOOK3 |

* The percentage of proteins in the group from the total number of potential protein targets of PLpro (61 proteins).

tor antagonist of the second type, suppressed SARS-CoV-2 replication by 50% ($EC_{50}$ was approximately 14 μM); however, inhibition of PLpro enzymatic activity was achieved at concentrations of the order of $10^{-4}$–$10^{-3}$ M [39]. It was found that compounds with antiproliferative activity CAS no. 331253-86-2, CAS no. 265312-55-8, and CAS no. 37854-59-4 inhibited PLpro with $IC_{50}$ values equal to 0.26, 0.39, and 0.53 μM, respectively [30]. However, only the CAS no. 37854-59-4 compound showed an acceptable level of viral replication suppression ($EC_{50}$ = 20 μM) [30].

## CYSTEIN RESIDUES IN PLpro AS TARGETS FOR SELECTIVE INHIBITORS

The zinc-binding domain in SARS-CoV-2 PLpro (Fig. 1) is represented by a "cysteine tetrad" (Cys189–X–X–Cys192–Xn–Cys224–X–Cys226), which coordinates the zinc ion. It is generally believed that sulfur-containing drugs active against PLpro, such as captopril or 6-thioguanine, can selectively "push out" zinc ions not only from PLpro but also from cellular proteins [40]. One of the successful solutions was implemented in peptidomimetics targeted at the cysteine residues of the PLpro active center. Examples were

**Table 2.** Position of potential protein partners of SARS-CoV PLpro and SARS-CoV-2 PLpro in the network of protein–protein interactions

| Data source | IMEx* | | STRINGdb** | |
|---|---|---|---|---|
| Proteins | Number of bonds | "betweenness centrality" | Number of bonds | "betweenness centrality" |
| MKRN2 | 3 | 436 | 1 | 0 |
| UFSP2 | 3 | 1249 | 5 | 2 |
| ZER1 | 5 | 1579 | 8 | 6055 |
| TRIM13 | 13 | 4819 | 0 | 0 |
| UFL1 | 13 | 3207 | 7 | 871 |
| USP3 | 26 | 14776 | 25 | 20083 |
| UBE2J1 | 28 | 10830 | 16 | 6028 |
| AUP1 | 36 | 14442 | 13 | 2280 |
| MKRN3 | 50 | 24427 | 0 | 0 |
| RCHY1 | 60 | 31175 | 23 | 20688 |
| FAF2 | 69 | 33358 | 49 | 38202 |

*International Molecular Exchange Consortium (www.imexconsortium.org); **Search Tool for the Retrieval of Interacting proteins database (https://string-db.org/).

**Table 3.** Parameters of the contact area of SARS-CoV PLpro and SARS-CoV-2 PLpro with cellular proteins

| Parameter/PD B ID* | Square, Å$^2$ | $H^+$ bonds | Salt bridges | S–S bonds | A.a.r. of PLpro involved in binding to cellular proteins |
|---|---|---|---|---|---|
| 4m0w | 999 | 17 | 4 | 0 | Leu163,** Gly164, Asp165, Glu168, Tyr265, Gly272, Glu162, Arg167, Gln175, Tyr268 |
| 5tl7 | 817 | 12 | 5 | 0 | |
| 6xaa | 945 | 17 | 7 | 0 | Gly163, Asp164, Arg166, Glu167, Tyr264, Gly271, Glu161, Leu162, Ser170, Glu203, Met208, Thr225, Tyr268, Tyr269 |
| 6xa9 | 804 | 11 | 4 | 0 | |

*The parameters of the contact area of the crystallographic models were determined on the PDBePISA server (https://www.ebi.ac.uk/pdbe/pisa/). 3D models: 4m0w and 5tl7—SARS-CoV PLpro/ubiquitin and PLpro/ISG-15, respectively; 6xaa and 6xa9—SARS-CoV-2 PLpro/ubiquitin and PLpro/ISG-15, respectively; ** Conservative a.a.r. are underlined.

the irreversible inhibitors VIR250 and VIR251, which form a covalent thioester bond with the PLpro cysteine residue at position 111 [41].

## DOUBLE-ACTING INHIBITORS TARGETING PLpro AND Mpro

An analysis of the studies in search of compounds capable of inhibiting both SARS-CoV-2 proteases at once revealed a number of candidate compounds with a certain pharmacological potential. One of the chalcone derivatives (compound 6, Fig. 2f) inhibited Mpro and PLpro with $IC_{50}$ values equal to 11 and 1 μM, respectively [22]. Ginkgolic and anacardic acids suppressing SARS-CoV-2 replication were identified as irreversible inhibitors of Mpro and PLpro with $IC_{50}$ of 2 and 16 μM, respectively; when dithiotreitol was added, the $IC_{50}$ values did not change [21]. Compound 29 suppressing virus replication ($EC_{50}$ approximately 1 μM) inhibited both SARS-CoV-2 proteases with $IC_{50}$ 0.67–1.72 μM and $K_D$ above 25 μM. Molecular docking showed two possible variants of binding of compound 29 in the active center, noncovalent and covalent, which indicates the mechanism of irreversible inhibition in the latter case [23]. Twenty-three derivatives of ebselen, which has anti-inflammatory, antioxidant, and cytoprotective activity, showed a differential spectrum of inhibition of PLpro and Mpro SARS-CoV-2 in the range from $10^{-8}$ to $10^{-6}$ M [24].

## PLpro INHIBITORS OF PEPTIDE NATURE

Pharmacologically active agents of a peptide nature targeting proteins of the SARS-CoV-2 replication apparatus are of considerable interest for the development of antiviral drugs, primarily from the point of view of convenience of organic synthesis [42]. The literature describes the results of preclinical studies of a

**Table 4.** Prediction of amino acid residues of SARS-CoV-2 PLpro involved in the binding of natural compounds

| No. | Compound name | $M_r$ | CAS No. | Amino acid residues |
|---|---|---|---|---|
| 1 | (–)-Epigallocatechin gallate | 458 | 989515 | ASP164, GLY266, TYR268, TYR273 |
| 2 | Calceolarioside B | 478 | 105471985 | LYS157, LEU162, ASP164, ALA246, GLY266, TYR273 |
| 3 | Chebulagic acid | 954 | 23094715 | GLY163, ASP164, ARG166, GLU167, GLY266, TYR268, TYR 273 |
| 4 | Corilagin | 634 | 23094691 | LYS157, GLY163, ASP164, GLU167, TYR273 |
| 5 | Forsythoside A | 624 | 79916771 | LYS157, ASP164, ARG166, GLU167, TYR264, GLY266, TYR273 |
| 6 | Ganoderiol F | 454 | 114567474 | LYS157, ASP164, ARG166, TYR264, ASN267, ASP302 |
| 7 | Glycyrrhizic acid | 819 | – | LEU162, ASP164, ARG166, GLU167, TYR264, TYR268, TYR273 |
| 8 | Hinokiflavone | 538 | 19202369 | LEU162, ARG166, TYR273 |
| 9 | Mulberrofuran G | 562 | 87085005 | LEU162, ARG166, TYR273 |
| 10 | Mulberroside C | 458 | 102841430 | LYS157, LEU162, GLY163, ARG166, TYR273 |
| 11 | Myriceric acid B | 634 | 55497795 | LYS157, ARG166, TYR273 |
| 12 | Procyanidin B1 | 578 | 29106512 | GLY163, ASP164, ARG166, GLY266, TYR264, TYR273 |
| 13 | Sennoside A | 862 | 81276 | LYS157, LEU162, ASP164, TYR268, TYR273 |

prophylactic vaccine preparation for intranasal administration with a short duration of action based on a lipopeptide, blocking the interaction of SARS-CoV-2 with susceptible cells [43]. It is worth saying that reports on peptide inhibitors of SARS-CoV-2 PLpro are much less common compared to low-molecular compounds of a nonpeptide nature. In addition to purely bioinformatic prediction of such peptides [44, 45], there are studies with experimental verification of computer predictions. As an example, the authors of [46] created constructions based on the LRGG motif of recognition of PLpro, cross-linked by a chemical linker with a GRL0617 inhibitor ($IC_{50}$ of the order of $10^{-6}$ M). It was shown in [47] that dimeric modified derivatives of peptides based on the bothropstoxin I motif (KKYRYHLKPFCKK) suppressed SARS-CoV-2 replication ($EC_{50}$ = 28–65 μM) and more specifically inhibited PLpro ($IC_{50}$ = 1.0–3.5 μM) in comparison with Mpro. The results of computer modeling made it possible to create models of binding of peptide inhibitors to PLpro in the BL2 region of the loop (265-TGNYQCG-271), which is critical for substrate recognition and binding of known low-molecular inhibitors [47].

## PROTEIN–PROTEIN INTERACTIONS INVOLVING PLpro AS TARGETS FOR PHARMACOLOGICAL EFFECTS

The interaction of viral proteins with cellular proteins plays a significant role in the pathogenesis of the disease since it can reprogram natural processes to maintain the life cycle of the virus. At the moment, there are quite a lot of results of interactomic profiling of potential protein partners of SARS-CoV-2 viral proteins. The analysis of eight articles [20, 48–54] allowed us to extract 472 cellular protein partners of PLpro. However, we included 61 proteins in the target group, which were found in two or more articles. A functional analysis of the entire spectrum of potential protein partners of PLpro is given in Table 1. Most proteins are located in the cytoplasm and in the membranes of the endoplasmic reticulum. They perform both structural (for example, binding to microtubules, macromolecules, and phospholipids) and enzymatic functions (for example, ligase activity). Next, the bioinformatic hypothesis was tested as to whether the cellular proteins binding to PLpro of coronaviruses SARS-CoV-2 and SARS-CoV are targets for exogenous proteins appearing in cells during infection or replication by other viruses. The search for such interactomic data and visualization of the PPI network were performed using the Virhostome resource (http://interactome.dfci.harvard.edu/V_hostome/) [55] on the examples of human papillomavirus, Epstein–Barr virus, and adenovirus (Fig. 3). It follows from Fig. 3 that at least approximately one third of the cellular proteins (23 of 61 proteins) interacting with PLpro are targets for proteins of other viruses, which may indicate the "universality" of the choice of cellular targets among these three viruses and coronaviruses SARS-CoV-2 and SARS-CoV. This follows from the fact that several different viral proteins, including PLpro, interact with one cellular target (for example, MBOAT7, Fig. 3). On the other hand, the HPV6B-E5A viral protein interacts with six different cellular proteins (FAF2, VMP1, AUP1, SNX19, TMEM43, and ARL6IP5) (Fig. 3). Thus, it can be assumed that, if the area of contact of a viral protein with cellular proteins is represented by

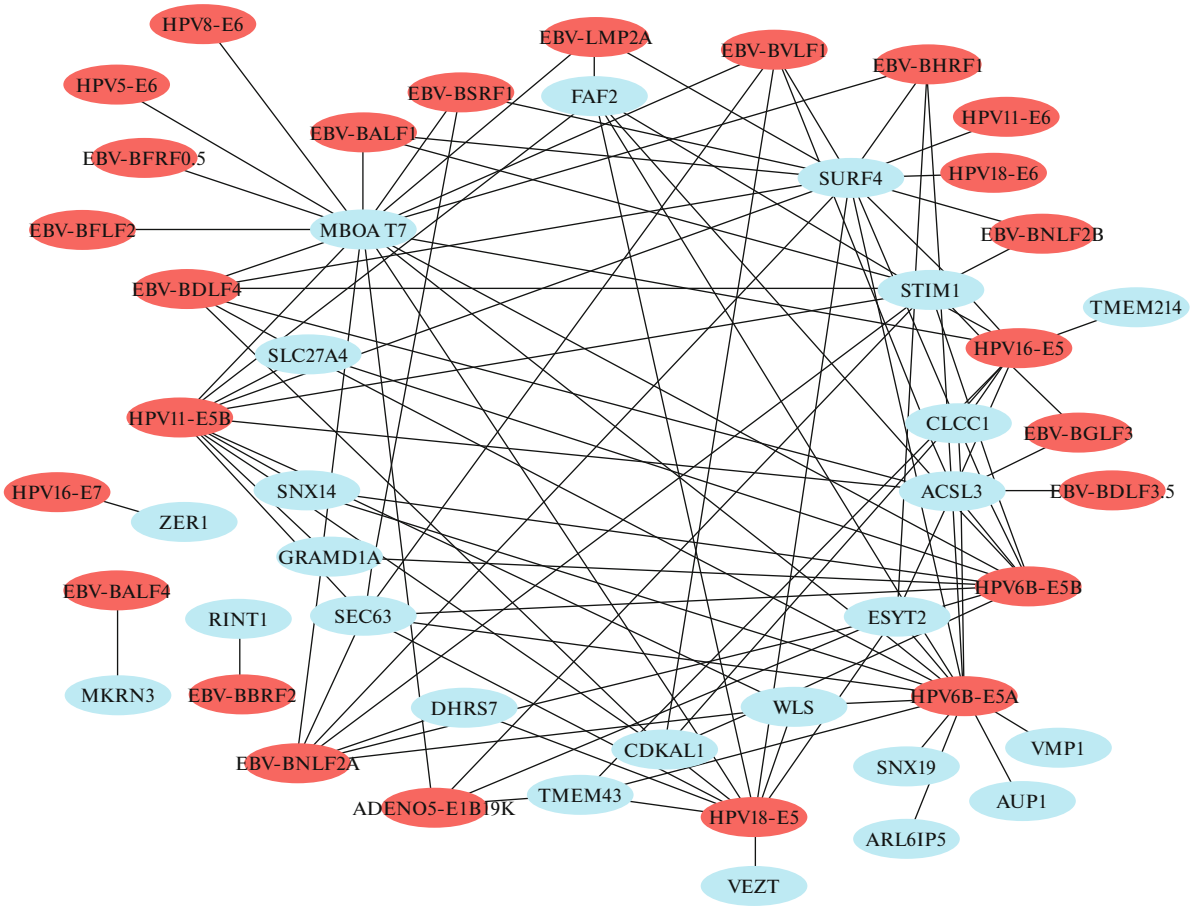


**Fig. 3.** Repertoire of cross-protein–protein interactions involving cellular proteins that can interact with SARS-CoV PLpro (blue color), with proteins of human papillomavirus (HPV), Epstein–Barr virus (EBV) and adenovirus (ADENO) according to the Virhostome resource. A list of 61 potential protein targets of PLpro was used as a search query.

the same structural element, it can be considered as a target for targeting pharmacologically active PPI inhibitors.

Eleven potential protein partners (MKRN2, MKRN3, RCHY1, FAF2, AUP1, TRIM13, UBE2J1, UFSP2, UFL1, USP3, and ZER1) interacting with SARS-CoV-2 PLpro and SARS-CoV are involved in the processes of ubiquitinylation and deubiquitinylation. This is in good agreement with the crystallographic data on the binding of PLpro with ubiquitin and ISG15 protein [56–58] and the presence of PLpro deubiquitinase activity. A PPI network involving 61 vertices (cellular protein targets of PLpro) was modeled in the NetworkAnalyst v 3.0 program [59] (https://www.networkanalyst.ca/) using IMEx (International Molecular Exchange Consortium) and STRINGdb (Search Tool for the Retrieval of Interacting proteins database) as data sources. For each of the 11 vertices (target proteins) in the PPI network (Table 2), data are given on the number of connections of a particular vertex with other vertices in the network and the "betweenness centrality," which indicates the number of shortest paths passing through the vertex [60]. It can be seen from the Table 2 that ubiquitin–protein ligases RCHY1 and FAF2, as well as deubiquitinases USP3 and UBE2J1, are the proteins with the largest number of connections in the PPI network; therefore, the interaction of viral proteins with them can lead to changes in the architecture of a significant part of the PPI network.

There are no crystallographic models of the interaction of PLpro with cellular proteins to date, with the exception of ubiquitin and ISG-15 protein; therefore, the concept of PPI modulation with the participation of PLpro by low-molecular compounds will be considered further on these two proteins. Although the amino acid sequences of PLpro of SARS-CoV and SARS-CoV-2 are highly homologous, the analysis of the contact areas of PLpro with ubiquitin or ISG-15 was performed for both viral proteases. It follows from Table 3 that most of the hydrogen bonds and salt bridges in the contact area are formed by conservative amino acid residues (a.a.r.) 163–170 and 265–273 of PLpro. Virtual screening of potential PPI inhibitors capable of binding in the area of contact between PLpro and ubiquitin (or ISG-15) was performed on

the ezCADD computer drug design platform among 154 low-molecular compounds of natural origin with established antiviral activity (catalog no. BCL0032, BioCrick Co., Ltd, PRC) [61]. The best models of PLpro binding with 13 compounds (455–954 Da) were predicted in a 20 × 25 × 20 box with center coordinates ($X = 0$, $Y = 72$, $Z = 40$) and selected by "score" values less than –8.0. Hydrogen bonds between compounds and a.a.r. of SARS-CoV-2 PLpro are shown in Table 4. The frequency of occurrence of a.a.r. of PLpro, significant for its interaction with low molecular mass compounds, was 92% (TYR273), 69% (ASP164 and ARG166), 54% (LEU162 and LYS157), and 31% (GLY163, GLU167, TYR264, GLY266, and TYR268). At the same time, GLY163, ASP164, ARG166, GLU167, and TYR264 of SARS-CoV-2 PLpro were involved in interaction with ubiquitin and ISG-15 (Table 3). The results of computer modeling in one of the studies indicated that the compound (-)-epigallocatechingalate forms hydrogen bonds with the residues of ASP164 and TYR273 of PLpro, which is comparable with the docking data (Tables 3, 4); at a concentration of 100 μM this compound slightly (by 13%) reduced the activity of PLpro [62]. However, it was found that (–)-epigallocatechingalate also binds to Mpro ($K_D = 6$ μM) with a more pronounced inhibitory effect ($IC_{50} = 0.8$ μM) [63].

The binding of low molecular mass compounds with a.a.r. of PLpro in the area of contact with ubiquitin should hinder the access of the substrate to the active center and inhibit the deubiquitinylation of cellular proteins. An example of a binding model with such a compound (corilagin) is shown in Fig. 4. As can be seen from the figure, corilagin binds to the active center of PLpro directly in the contact area of the protease with ubiquitin, while the "score" value is –10.0 (according to ezCADD) and the interaction energy is –7.58 kcal/mol (according to SwissDock) [64]. It can also be seen from Tables 3 and 4 that corilagin (according to the binding model) in this position can form hydrogen bonds with the conservative a.a.r. Gly163, Asp164 and Glu167 of PLpro, which are involved in the binding of ubiquitin. Thus, this low molecular mass compound can inhibit the deubiquitinase activity of PLpro by creating steric difficulties for ubiquitin binding and access of the polypeptide chain to the active center of PLpro. It is interesting to note that corilagin was previously identified as a blocker of the interaction of the SARS-CoV-2 spike protein with the ACE2 receptor on the cell surface [65]. The effect of pharmacologically active compounds on the contact area of PLpro with ubiquitin and ISG-15 may be an additional antiviral strategy, blocking the possibility of the virus to disrupt the natural reaction of the cell to its presence. Inhibitors of protein complexation binding outside the area of the PLpro active center indirectly affect proteolytic activity [66]. The latter is also relevant in the light of study [31], in which in silico models of the binding of SARS-CoV-2 PLpro with three compounds, EACC, KY-226, and tropifexor ($IC_{50}$ of the order of $10^{-6}$–$10^{-5}$ M), in the U-shaped pocket of the protease (also the binding site of the control inhibitor GRL0617) showed the involvement of a.a.r. GLN269, ASP164, TYR268, and LYS157 in complexation. Thus, Plpro SARS-CoV-2 can participate in interaction with at least 61 cellular proteins, which follows from the systematization of interactomic information according to several publications; however, crystallographic models exist only for two complexes to date: PLpro/ubiquitin and PLpro/ISG-15. Consequently, the question remains unexplored whether the binding site of these two proteins on PLpro is unique or characteristic of the positioning of other potential protein partners. What is the benefit of blocking the ubiquitin binding site with small molecule compounds with a wide spectrum of antiviral activity, such as corilagin, and suppressing the deubiquitinase activity of PLpro? It is known that viral deubiquitinases target several cellular processes, mainly various molecules involved in the signaling pathway of innate immunity, thereby indirectly suppressing it and stimulating viral replication [67, 68]. These events are due to several causes: deubiquitinylation of TRAF3 and TRAF6 proteins (factors associated with the TNF receptor) with subsequent violations of the interferon signaling pathway and the production of proinflammatory cytokines; inactivation of the pathway involving Toll-like receptors and the universal transcription factor NF-kB, which regulates the expression of immune response genes, including the interferon-beta gene; PCNA (nuclear antigen of proliferating cells)-associated blockade of recruitment of Nu DNA polymerase to DNA damage sites and some other causes [67, 68].

## CONCLUSIONS

Discovery of new specific inhibitors of viral SARS-CoV-2 proteases Mpro and PLpro is an extremely dynamic and highly competitive area of development among many scientific groups in the world. Most experimentally verified inhibitors target the active center of SARS-CoV-2 proteases. In this study, we analyzed a number of promising PLpro inhibitors and identified at least six compounds with a favorable pharmacokinetic profile and high inhibition potential according to $IC_{50}$ and $EC_{50}$ values, which can be used as basic structures to create more specific and effective candidate antiviral drugs. But as the authors of [69] rightly point out, despite encouraging progress in identifying at least 70 structures of PLpro inhibitors over the past 2 years, there is still a long way to go for the introduction of inhibitors into clinical practice. To date, it has not been shown that rationally developed PLpro inhibitors have antiviral efficacy in vivo against SARS-CoV-2 infection in animal models.

The systematization of data on interactomic profiling of protein–protein interactions involving PLpro

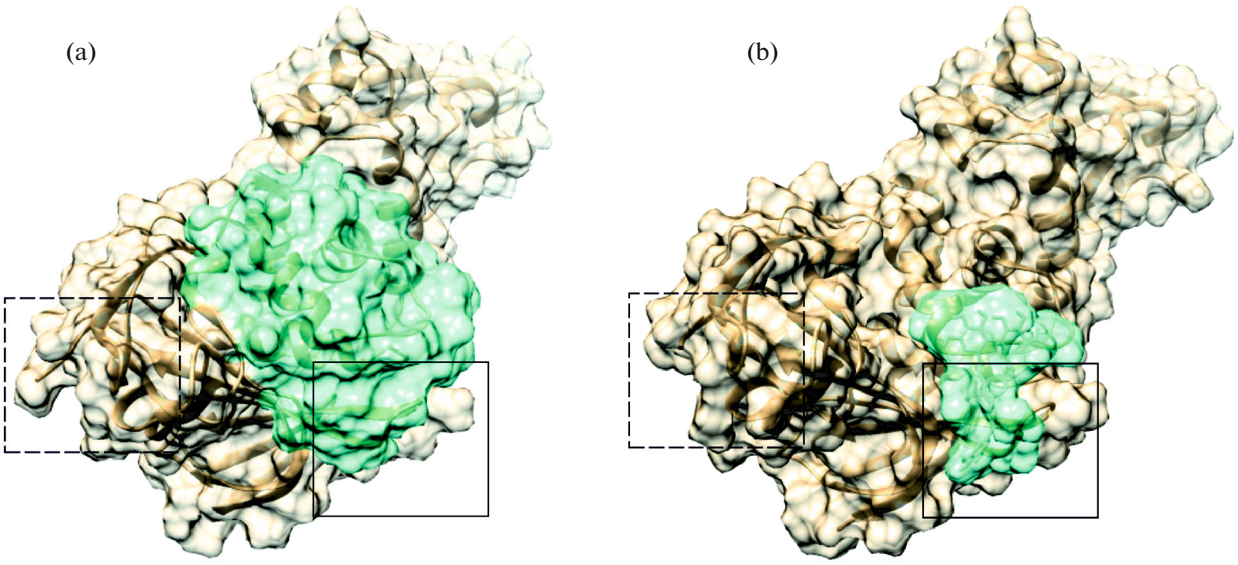


**Fig. 4.** (a) Visualization of a 3D model of the SARS-CoV-2 PLpro complex and ubiquitin (PDB ID 6xaa [56], resolution 2.70 Å, 8.5 kDa). (b) A model of docking of a low molecular mass compound of corilagin (630 Da) into the contact area of SARS-CoV-2 PLpro and ubiquitin (PDB ID: 6wrh [5], resolution 1.60 Å). Solid and dotted frames highlight the areas of the active center and the Zn-binding domain, respectively.

and cellular proteins allowed us to identify 11 cellular proteins involved in the processes of ubiquitinylation and deubiquitinylation. We believe that the selection of pharmacologically active agents targeting peripheral PLpro sites, such as the contact area of PLpro and cellular proteins, may be an alternative option for antiviral effect on SARS-CoV-2.

## FUNDING

The work was carried out within the framework of the Program of Fundamental Scientific Research in the Russian Federation for the long-term period (2021–2030), project no. 122030100168-2.

## COMPLIANCE WITH ETHICAL STANDARDS

*Conflict of interest*. The authors declare that they have no conflicts of interest.

*Statement of the welfare of humans or animals*. The article does not contain any studies involving humans or animals in experiments performed by any of the authors.

## REFERENCES

1. R. Ganesh, K. Mahalingam, N. Kandaswamy, et al., Indian J. Public Health **65**, 375 (2021).
2. R. M. Barber, R. J. D. Sorensen, D. M. Pigott, et al., Lancet **399**, 2351 (2022).
3. M. Mei and X. Tan, Front. Mol. Biosci. **8**, 671263 (2021).
4. Y. M. Báez-Santos, S. E. St John, and A. D. Mesecar, Antiviral Res. **115**, 21 (2015).
5. J. Osipiuk, S.-A. Azizi, S. Dvorkin, et al., Nat. Commun. **12**, 743 (2021).
6. X. Gao, B. Qin, P. Chen, et al., Acta Pharm. Sin. B **11**, 237 (2021).
7. A. Stasiulewicz, A. W. Maksymiuk, M. L. Nguyen, et al., Int. J. Mol. Sci. **22**, 3957 (2021).
8. D. Li, J. Luan, and L. Zhang, Biochem. Biophys. Res. Commun. **538**, 72 (2021).
9. S. Rajpoot, M. Alagumuthu, and M. S. Baig, Curr. Res. Struct. Biol. **3**, 9 (2021).
10. C. Wu, Y. Liu, Y. Yang, et al., Acta Pharm. Sin. B **10**, 766 (2020).
11. P. Delre, F. Caporuscio, M. Saviano, et al., Front. Chem. **8**, 594009 (2020).
12. M. Loffredo, H. Lucero, D.-Y. Chen, et al., Sci. Rep. **11**, 5433 (2021).
13. C. Ma and J. Wang, ACS Pharmacol. Transl. Sci. **5**, 102 (2022).
14. H. Shan, J. Liu, J. Shen, et al., Cell Chem. Biol. **28**, 855 (2021).
15. Z. Shen, K. Ratia, L. Cooper, et al., J. Med. Chem. **65**(4), 2940 (2022).
16. D. Shin, R. Mukherjee, D. Grewe, et al., Nature **587**, 657 (2020).
17. N. Barretto, D. Jukneliene, K. Ratia, et al., J. Virol. **79**, 15189 (2005).
18. S. G. Devaraj, N. Wang, Z. Chen, et al., J. Biol. Chem. **282**, 32208 (2007).
19. X. Chen, X. Yang, Y. Zheng, et al., Protein Cell **5**, 369 (2014).
20. A. Stukalov, V. Girault, V. Grass, et al., Nature **594**, 246 (2021).
21. Z. Chen, Q. Cui, L. Cooper, et al., Cell Biosci. **11**, 45 (2021).

22. J.-Y. Park, J.-A. Ko, D. W. Kim, et al., J. Enzyme Inhib. Med. Chem. **31**, 23 (2016).

23. V. Di Sarno, G. Lauro, S. Musella, et al., Eur. J. Med. Chem. **226**, 113863 (2021).

24. M. Zmudzinski, W. Rut, K. Olech, et al., bioRxiv 2020.08.30.273979 (2020). https://doi.org/10.1101/2020.08.30.273979

25. C. Ma, Y. Hu, J. A. Townsend, et al., ACS Pharmacol. Transl. Sci. **3**, 1265 (2020).

26. Y. Zhao, X. Du, Y. Duan, et al., Protein Cell **12**, 877 (2021).

27. C.-J. Kuo, T.-L. Chao, H.-C. Kao, et al., Antimicrob. Agents Chemother. **65**, e02577 (2021).

28. Z. Xia, M. D. Sacco, C. Ma, et al., ACS Cent. Sci. **7**, 1245 (2021). https://doi.org/10.1021/acscentsci.1c00519

29. B. T. Freitas, I. A. Durie, J. Murray, et al., ACS Infect. Dis. **6**, 2099 (2020).

30. C. T. Lim, K. W. Tan, M. Wu, et al., Biochem. J. **478**, 2517 (2021).

31. C. Ma, Y. Hu, Y. Wang, et al., ACS Infect. Dis. **8** , 1022 (2022).

32. B. Sanders, S. Pohkrel, A. Labbe, et al., Res. Square (2021). https://doi.org/10.21203/rs.3.rs-906621/v1

33. D. Gfeller, A. Grosdidier, M. Wirth, et al., Nucleic Acids Res. **42**, W32 (2014).

34. M. K. Gilson, T. Liu, M. Baitaluk, et al., Nucleic Acids Res. **44** (D1), D1045 (2016).

35. Z.-J. Yao, J. Dong, Y.-J. Che, et al., J. Comput.-Aided Mol. Des. **30**, 413 (2016).

36. A. Daina, O. Michielin, and V. Zoete, Sci. Rep. **7**, 42717 (2017).

37. C.-C. Cho, S. G. Li, T. J. Lalonde, et al., ChemMedChem **17**, e202100455 (2022).

38. M. A. Redhead, C. D. Owen, L. Brewitz, et al., Sci. Rep. **11**, 13208 (2021).

39. R. Nejat, A. S. Sadr, B. Freitas, et al., J. Pharm. Pharm. Sci. **24**, 390 (2021).

40. B. K. Maiti, ACS Pharmacol. Transl. Sci. **3**, 1017 (2020).

41. W. Rut, Z. Lv, M. Zmudzinski, et al., Sci. Adv. **6**, eabd4596 (2020).

42. A. S. Skwarecki, M. G. Nowak, and M. J. Milewska, ChemMedChem **16**, 3106 (2021).

43. R. D. de Vries, K. S. Schmitz, F. T. Bovier, et al., Science **371**, 1379 (2021).

44. M. Moradi, R. Golmohammadi, A. Najafi, et al., Int. J. Pept. Res. Ther. **28**, 24 (2022).

45. S. Sasidharan, C. Selvaraj, S. K. Singh, et al., J. Biomol. Struct. Dyn. **39**, 5706 (2021).

46. N. Liu, Y. Zhang, Y. Lei, et al., J. Med. Chem. **65**, 876 (2022).

47. M. C. L. C. Freire, G. D. Noske, N. V. Bitencourt, et al., Molecules **26**, 4896 (2021).

48. J. Li, M. Guo, X. Tian, et al., Med **2**, 99 (2021).

49. E. M. N. Laurent, Y. Sofianatos, A. Komarova, et al., bioRxiv 2020.08.28.272955 (2020). https://doi.org/10.1101/2020.08.28.272955

50. P. Samavarchi-Tehrani, H. Abdouni, J. D. R. Knight, et al., bioRxiv 2020.09.03.282103 (2020). https://doi.org/10.1101/2020.09.03.282103

51. J. R. St-Germain, A. Astori, P. Samavarchi-Tehrani, et al., bioRxiv 2020.08.28.269175 (2020). https://doi.org/10.1101/2020.08.28.269175

52. D.-K. Kim, B. Weller, C.-W. Lin, et al., Nat. Biotechnol. **41**, 140 (2022). https://doi.org/10.1038/s41587-022-01475-z

53. S. Pfefferle, J. Schöpf, M. Kögl, et al., PLoS Pathog. **7**, e1002331 (2011).

54. Z. Chen, C. Wang, X. Feng, et al., EMBO J. **40**, e107776 (2021).

55. O. Rozenblatt-Rosen, R. C. Deo, M. Padi, et al., Nature **487**, 491 (2012).

56. T. Klemm, G. Ebert, D. J. Calleja, et al., EMBO J. **39**, e106275 (2020).

57. C.-Y. Chou, H.-Y. Lai, H.-Y. Chen, et al., Acta Crystallogr., Sect. D **70**, 572 (2014).

58. C. M. Daczkowski, J. V. Dzimianski, J. R. Clasman, et al., J. Mol. Biol. **429**, 1661 (2017).

59. G. Zhou, O. Soufan, J. Ewald, et al., Nucleic Acids Res. **47**, W234 (2019).

60. J. K. Das, S. Roy, and P. H. Guzzi, Infect. Genet. Evol. **93**, 104921 (2021).

61. A. Tao, Y. Huang, Y. Shinohara, et al., J. Chem. Inf. Model. **59**, 18 (2019).

62. E. Pitsillou, J. Liang, K. Ververis, et al., J. Mol. Graphics Modell. **104**, 107851 (2021).

63. A. Du, R. Zheng, C. Disoma, et al., Int. J. Biol. Macromol. **176**, 1 (2021).

64. A. Grosdidier, V. Zoete, and O. Michielin, Nucleic Acids Res. **39**, W270 (2011).

65. L. J. Yang, R. H. Chen, S. Hamdoun, et al., Phytomedicine **87**, 153591 (2021).

66. H. Lee, H. Lei, B. D. Santarsiero, et al., ACS Chem. Biol. **10**, 1456 (2015).

67. Q. Zhang, Q. Jia, W. Gao, et al., Front. Microbiol. **13**, 839624 (2022).

68. S. M. Soh, Y. J. Kim, H. H. Kim, et al., Int. J. Mol. Sci. **23**, 492 (2022).

69. H. Tan, Y. Hu, P. Jadhav, et al., J. Med. Chem. **65**, 7561 (2022).

*Translated by E. Puchkov*